

Characterization of Steel-Ta Dissimilar Metal Builds Made Using Very High Power Ultrasonic Additive Manufacturing (VHP-UAM)



NIYANTH SRIDHARAN, MARK NORFOLK, and SUDARSANAM SURESH BABU

Ultrasonic additive manufacturing is a solid-state additive manufacturing technique that utilizes ultrasonic vibrations to bond metal tapes into near net-shaped components. The major advantage of this process is the ability to manufacture layered structures with dissimilar materials without any intermetallic formation. Majority of the published literature had focused only on the bond formation mechanism in Aluminum alloys. The current work pertains to explain the microstructure evolution during dissimilar joining of iron and tantalum using very high power ultrasonic additive manufacturing and characterization of the interfaces using electron back-scattered diffraction and Nano-indentation measurement. The results showed extensive grain refinement at the bonded interfaces of these metals. This phenomenon was attributed to continuous dynamic recrystallization process driven by the high strain rate plastic deformation and associated adiabatic heating that is well below 50 pct of melting point of both iron and Ta.

DOI: 10.1007/s11661-016-3354-5

© The Minerals, Metals & Materials Society and ASM International 2016

I. INTRODUCTION

ULTRASONIC Additive Manufacturing UAM is a solid-state processing technique that uses ultrasonic vibrations to bond metal tapes into near net-shaped components. A metal tape is initially bonded to a substrate material with additional tapes being subsequently bonded to the previous layer.^[1] Ultrasonic vibrations of 20 kHz are locally applied to the metal foils through a sonotrode under a static normal force.^[2] However, due to the limited power input (1.5 kW) of the conventional UAM system, adequate and consistent bonding is not achieved.^[9] This shortcoming is addressed with the development of the very high power ultrasonic additive manufacturing (VHP-UAM) with greater ultrasonic power (9 kW). High power is realized through larger vibration amplitudes (52 μm as against 26 μm in the conventional UAM) and higher normal force levels (15 kN as against 2 kN in the conventional UAM). A machine delivering up to 9 kW of power at 20 kHz resonant frequencies has been developed by Fabrisonics.^[9] The effect of the process parameters such as normal force, amplitude and travel speed on the bond quality has been investigated in detail using mechanical tests such as shear and transverse tensile testing^[3] and

using the concept of linear weld density (LWD). The LWD is the ratio of the bonded interface to the total length of the interface and is measured using an optical microscope.^[4,5] It has been shown that the LWD and bond strength is related directly to the sonotrode horn texture.^[1] Apart from the LWD, mechanical strength of these bonds also related to extent of metallurgical bonding between the foils.^[3]

Microstructural evolution is the key to understand the extent of metallurgical bonding. Work on VHP-UAM has been concentrated mostly on FCC metals. Recent publications indicate that the bond formation occurs due to complex interactions of many phenomena including mechanical interlocking due to plastic deformation,^[6] frictional heating, deformation heating, recrystallization, diffusion, and contact between nascent surfaces.^[2] Extensive microscopy conducted on the Aluminum builds using dual beam FIB in conjunction with TEM revealed that the microstructure at the interfaces are affected by severe plastic deformation (SPD) of bulk (5 μm) resulting in the grain refinement (0.5 μm to few nanometers).^[1,7] The above observation confirms that the UAM process affects only the grains at the interface and does not have any major long-range effects into the bulk of materials. David Schick calculated the strain rate at the interface during deformation to be close to 10^5 s^{-1} .^[8] In order to understand the microstructure and texture evolution at the interface was measured using EBSD^[1,2,8] and these results indicate large misorientation of the grains at the interface indicative of newly formed grains. Sriraman *et al.* in their work on Cu^[9] observed softening at the interface along with the presence of equiaxed grains with high angle grain boundaries, similar to observations in Al-3003,^[2] and attributed these changes to dynamic

NIYANTH SRIDHARAN, formerly Graduate Student, and SUDARSANAM SURESH BABU, formerly Professor with the Department of Welding Engineering, The Ohio State University, Columbus 43221, are now with the Department of Mechanical Aerospace Biomedical Engineering, University of Tennessee, Knoxville 37916. Contact e-mail: sniyanth@vols.utk.edu, niyanth.sridharan@gmail.com MARK NORFOLK, President, is with Fabrisonic, Columbus 43221.

Manuscript submitted July 31, 2015.

Article published online February 24, 2016

recrystallization. This hypothesis was based on calculations that showed that the temperature rise due to adiabatic deformation exceeded $0.5 T_m$.^[9] Micro-texture data of Al-3003 build interfaces, obtained using EBSD, indicated a prominent shear texture $\{111\}$ $\langle 110 \rangle$ in comparison to the rolling texture of the bulk.^[2] Thermocouple measurements of the temperature at the Al-Al interface showed only a moderate rise in the temperature around 493 K (220 °C).^[8] The above phenomenon was attributed to the extensive deformation and collapse of the micro asperities at the interface followed by dynamic recrystallization brought about by the heat generated during deformation.^[2] Similar observations have been made during friction stir welding of Al alloys. In friction stir welds, the $\{111\}$ plane was roughly parallel to the direction of the pin and a $\langle 110 \rangle$ direction to the transverse direction of the plate. Since this orientation correlates well with critically resolved shear stress for slip, the correlation between texture development and plastic deformation was confirmed.^[10]

The motivation behind this work is to answer the question whether BCC materials also undergo similar dynamic recrystallization at the interface driven by the heat generated by the adiabatic plastic deformation process. Due to lack of any previous work with UAM, we embarked on a literature review with reference to deformation textures in BCC during severe plastic deformation (SPD)^[11] at high strain rate deformations. During friction stir welding, which relies on high strain rate deformation, shear textures was observed by Minorov *et al.*^[12] Shear texture was also observed during friction stir processing of pure Iron.^[12] These authors observed a fine grain structure with a low aspect ratio along with significant dislocation density.^[12] Similarly nano structured grains were also obtained after severe plastic deformation (*e.g.*, high pressure torsion) processes at high strain rate at ambient temperatures.^[13–16] The above grain structure evolution during high strain rate was correlated to grain subdivision mechanism. Based on the above SPD literature, because of the similar shear strain rate magnitudes, our hypothesis is that grain subdivision may be an alternative mechanism for bond formation in BCC metals, instead of dynamic recrystallization. We explored the above hypothesis in an industrially relevant dissimilar metal combination; Iron and tantalum sheets.

There has been significant interest in Ta over steel dissimilar metal joints, which finds applications as clads, in corrosive environments. Due to the high differences in the melting points of these metals [Ta: 3293 K (3020 °C) and Fe: 1811 K (1538 °C)], solid-state welding techniques (*e.g.*, explosive welding) is preferred instead of fusion welding. However, there is interest in using alternative solid-state joining techniques, because of the possibility of intermetallic formation at the interface during explosive welding.^[17] In addition UAM has the potential to fabricate complex geometries as well. Goals of the current work are two folds (i) evaluate the feasibility of UAM using small samples and (ii) obtain fundamental knowledge of microstructural evolution for aiding future scaling up of UAM to make large-scale structures.

II. EXPERIMENTAL WORK

The material used for this study was 99.5 pct pure Ta sheet 50 μm thick and 1010 steel substrate 2.5 mm thick. The tape was placed over the substrate and ultrasonic vibrations were applied through a rotating sonotrode, which was made of Ti-6Al-4V. In this work, the welding parameters were developed using trial and error and were not optimized for bond strength. The welds used for characterization were the ones where the foils could not be detached from the substrate. The parameters used for the fabrication of the builds were a normal load of 7000 N vibration amplitude of 36 μm and a travel speed of 15 mm/s. The total length of the weld was 4 inches (101.6 mm) and the width of the foil used was 1 inch (25.4 mm). The build was cut parallel the Normal Direction (ND) using a low cutting speed with a coolant to avoid heating so as to preserve the substructures developed during plastic deformation. The naming convention used for the presentation of the microstructural data is shown in Figure 1, *i.e.*, ND, TD, and VD represent normal direction, transverse direction, and vibration direction, respectively. The samples were mounted using conductive Bakelite and prior to polishing, the samples were ground with abrasive paper using water as a lubricant and mechanically polished with a final polishing step comprising a 1 μm diamond paste. A suitable finish for EBSD was obtained by chemical-mechanical polishing on the Buehler Vibromet vibratory polisher with a non-crystalline colloidal silica suspension.

Characterization was performed using Optical microscopy, SEM with EDS, Electron Backscatter Diffraction and Nano-indentation. The center of the builds were then analyzed using Scanning Electron microscopy and EBSD analysis was performed using a PHILIPS XL-30 FEG scanning electron microscope equipped with the TSL OIM EBSD system under 20 kV accelerating voltage and a 17-mm working distance. The electron beam was scanned with a step size of 0.05 μm in order to pick up small variations of misorientation within the grains. Hardness measurements were performed using a MTS Nano indenter XP at selected locations using load vs depth sensing techniques described elsewhere.^[18] The indentation was carried out using a 3-faced Berkovich indenter and to a depth of 500 nm at a strain rate of 0.05 s^{-1} and a dwell time of 20 seconds to remove the

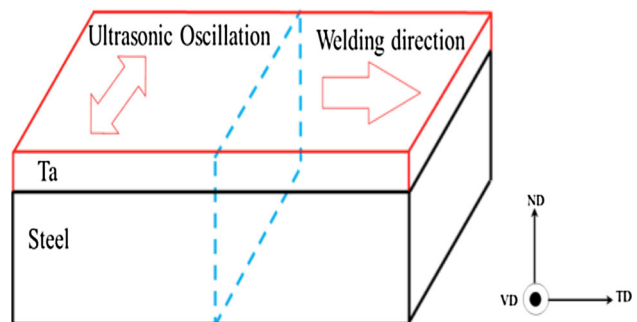


Fig. 1—Schematic illustration of build fabricated by VHP-UAM and specimens cut off from the build (indicated by a dotted line).

time-dependent plasticity effects. The adjacent indents where placed at a distance of 10 μm .

III. RESULTS

A. Scanning Election Microscopy and EDS of VHP-UAM Builds

A standard technique used to estimate the effectiveness of bonding is a linear weld density (LWD), which is the ratio of the length of the interface that appears to be bonded to the total length of the interface. Due to the inhomogeneity of the bonding process the LWD for this case was measured from a 6 different SEM images taken from random locations at a low magnification 50 times and the average LWD value was calculated. The LWD was 0.76 or 76 pct of the total area was bonded. The reason for the low LWD in this case is due to the fact that no detailed design of experiments was performed to maximize the linear weld density. Figures 2(a) and (b) show the interface characterized by SEM. The direction of the vibration of the sonotrode is marked on the images. There were regions where contact between the substrate and the foil has not occurred and regions where extensive plastic deformation had occurred. These features indicate heterogeneous bonding across the interfaces. The interface also had several wave-like features similar marked in Figure 2(b) similar to the features observed in samples joined by explosive welding.^[19] The dark regions marked by arrows in Figure 2(a) are voids indicating absence of contact between the substrate and foil. Across the interface are randomly dispersed voids in between bonded regions as shown in Figure 2(a). Several unbonded regions correlate well with lack of metal-to-metal contact. The above phenomenon has been correlated^[4] to heterogeneity of plastic deformation along the contact area of the sonotrode with the foil due to the differences in contact pressure. Several wave-like features were characterized

and Figure 2(b) shows a wavy interface (marked with arrows) associated with extensive plastic flow^[20] of the upper region of the foil. It also appears from Figure 2(b) that the tantalum has flowed around the “hills” and “valleys” of the steel asperities (marked by arrows). This phenomenon has also been observed on the upper region of the foils and has been hypothesized to form as a result of the imprint of sonotrode on the top region of the foil. Adjacent to the wave features “micro porosity” had also been observed at a distance of $\sim 8 \mu\text{m}$ from the interface and the size of these micro pores were around ~ 3 to $5 \mu\text{m}$. Similar “micro porosity” formation has also been previously observed in ultrasonic spot welds in areas made with higher energy. However, the micro-porosity observed in literature is due to excessive material flow, rather than lack of bonding. An EDS spectrum (Figure 3(b)) reveals oxygen peaks with strong iron and Ta peaks suggesting that the wear particles predominantly are broken off from the rubbing surfaces. The size of the wear debris was estimated to be from 2 to $10 \mu\text{m}$ based on optical microscopy.

In order to investigate the possibility of inter diffusion between the Ta and steel and to understand the breaking and dispersion of the oxides at the interface due to plastic flow, EDS maps were obtained from following locations: bonded region, wavy regions, and incomplete bonding area (see marked in Figure 4(a)). The maps show oxygen concentration at the unbonded interfaces. It is pertinent to mention that oxides were also observed in the aluminum UAM samples at Al-Al interfaces. Dehoff *et al.*,^[1] hypothesized that these oxide layers formed as a result of melting of the Al layers due to adiabatic heating at the interfaces. Although our micro-graphic images appear to indicate extensive mixing between the Ta and steel at the interface (see Figure 4(a)), EDS analyses did not shown any inter diffusion of Ta and Fe across the interfaces. Furthermore, interdiffusion of Fe into Ta is highly improbable due to the low solid solubility of Fe in Ta, *i.e.*, less than 2 at. pct at temperatures higher than 1073 K (800 °C).

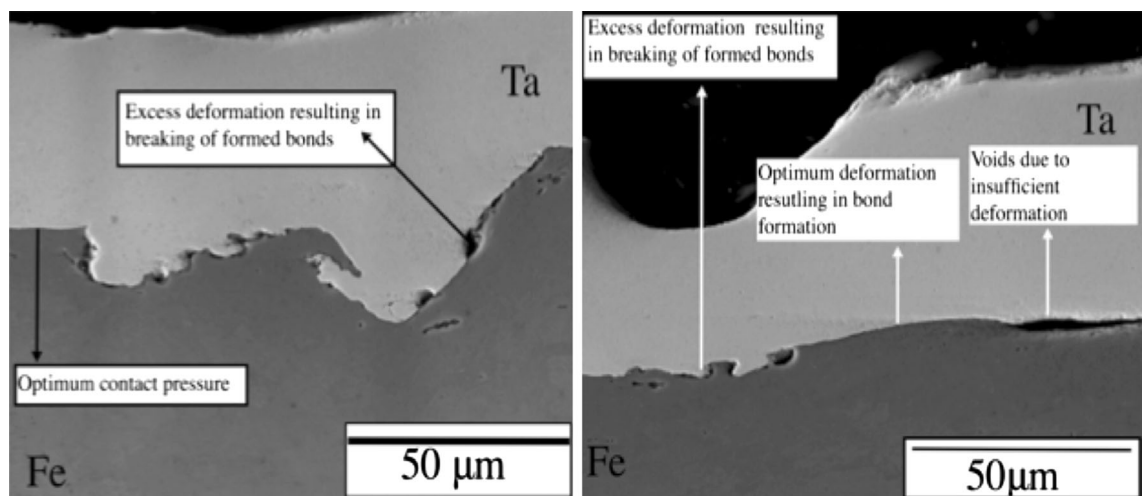


Fig. 2—(a) SEM image showing bonded regions voids and the waves (b) SEM image showing waves at the interface.

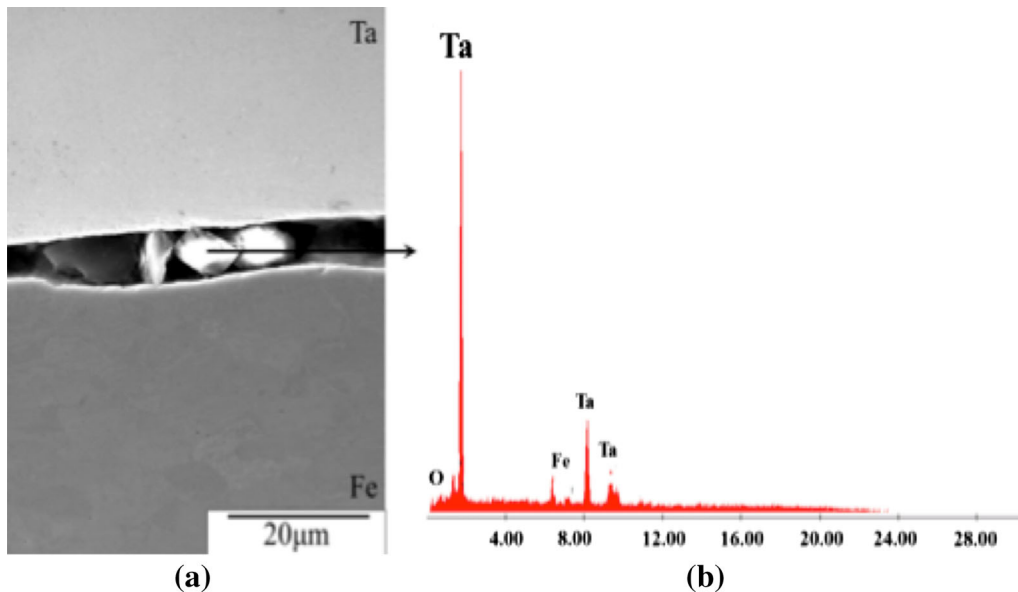


Fig. 3—SEM micrographs of the Ta steel interface. (a) Sliding debris. (b) EDS spectrum of the debris.

B. Orientation Imaging Microscopy (OIM) Using Electron Back-Scattered Diffraction (EBSD)

EBSD was performed to examine the detailed micro-texture and rationalize the deformation processes at three regions, *i.e.*, bonded region, wavy regions and incomplete bonding area. The microstructural characteristics of the non-bonded regions are shown in Figures 5(a) and (b). The image does not show any evidence for grain refinement or deformation. This observation is also confirmed by the grain-orientation-spread (GOS) map. The GOS is the average deviation between the orientation of each point in the grain and the average orientation of the grain. GOS analyses are usually performed to rationalize the extent and mechanisms of plastic deformation at the interfaces.^[21] GOS is sensitive to dislocation cells created during plastic deformation compared to inverse pole figures (IPF) of grain images. The dislocation cells within a parent grain will have small misorientation with the matrix and thereby will not be indexed as new grains. This is expected since the EBSD grain-grouping algorithm simply enforces that any two points which differ in orientation less than a specific tolerance levels are part of the parent grain surrounding them. In a deformed grain with dislocation cells, the point-to-point misorientation may not exceed the tolerance angle to be indexed as a new grain. In contrast, the GOS is even small misorientations arising due to geometrically necessary dislocations (GND's). In addition to GOS, image quality indicator (IQI) maps can also be used to understand the amount of stored energy due to deformation in the sample qualitatively. Larger deformation results in a lower image quality due to lattice distortion. In Figure 5(c), the image quality of the microstructure indicates minimal lattice deformations. Figure 5(c) shows a decrease in the IQI at the steel side of the interface indicating some amount of deformation (which

is marked) and corresponding increase in the grain orientation spread in the region shown in Figure 5(c).

The characteristics of the bonded regions are shown in Figure 6. Figures 6(c) and (d) correspond to the marked region in Figure 6(a) at a higher magnification and obtained using a finer step size (5 nm) to detect small misorientations at the interface. The grains in the interface were equiaxed in nature with high angle grain boundaries as shown in Figure 6(c). The black regions marked in Figure 6(c) are present even in regions where it appeared to have physical continuity. However, EBSD patterns obtained from these regions could not be indexed. Figures 6(b) and (d) show a gradual increase in the amount of grain orientation spread at the interface indicating high concentrations of geometrically necessary dislocations. It is pertinent to note that in the fine-grained interface several grains are elongated with a comparatively high Grain orientation spread while several grains have a GOS close to 0 deg. There are some grains that have a GOS close to 4 deg showing that these grains with larger GOS have residual geometrically necessary dislocations (GND's). Geometrically necessary dislocations form due the activation of different slip systems on each side of the grain, which is strongly correlated to the initial orientation of the grain itself.^[22]

The misorientation profiles of an equiaxed grain (marked grain-2 in Figure 6(c)) and a grain at the sub-surface (marked grain-1 in Fig. 6(c)) of the interface are extracted for comparison. The plot shows the misorientation changes as a function of the normalized distance. The grain at the interface (grain-2) showed a very low misorientation distribution. In contrast, the data from grain-1 indicates several peaks and the spacing between the peaks are of the order of the grain size of the equiaxed zone of the interface. A detailed account of this mechanism is presented in the

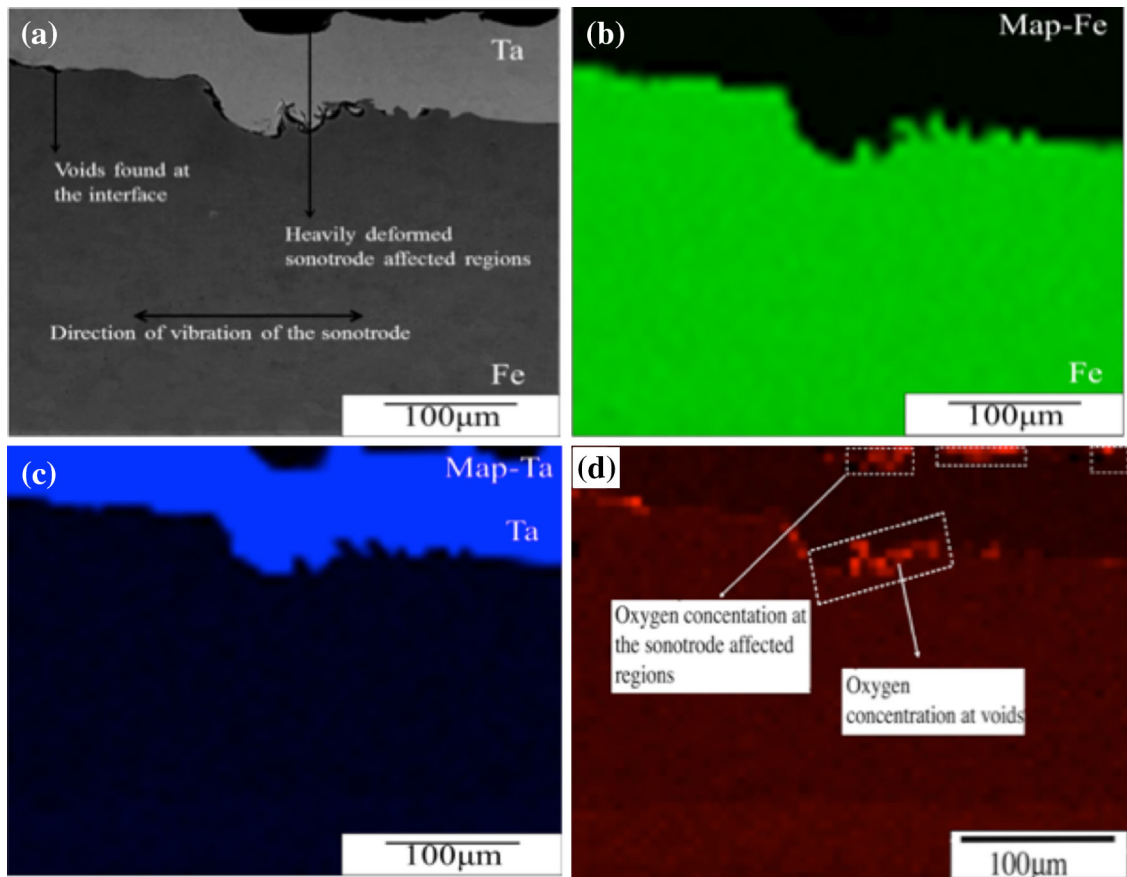


Fig. 4—EDS maps show oxygen concentration at the interface and in the sonotrode-affected regions.

discussions section. The grain size was calculated and the average grain size of the equiaxed grains at the interface was 125 nm showing the presence of nano crystalline grains at the interface.

Another region where there was excessive deformation and the formation of a “wavy interface” was characterized using EBSD and the IPF and the GOS analyses (see Figure 7). The interface showed a fine-grained structure similar to bonded regions. The GOS maps confirmed the onset of intense deformation close to the interface. The dark un-indexed regions could not be indexed. The misorientation profiles of individual grains were also extracted for analysis from the Ta grain close to the interface (grain-3), steel grain close to the interface (grain-1), and a steel grain in the substrate (grain-2) for analysis (see Figure 7(b)). The grain sizes here are much finer than those in the bonded regions.

The misorientation distribution of the grains showed peaks and the distance between certain peaks with high misorientations is of the order of the grain sizes at the interface. This is similar to what had been observed in the bonded region, which supports similar deformation mechanisms for grain refinement on both cases. The misorientation distribution of the Ta and the steel grains at the interface reveals that the average misorientation is much higher in the Ta grain than the steel grain. This suggests higher extent of plastic strain in the Ta foil.

This is expected considering the high purity of Ta foil used in this study. Often the reduction interstitial concentration is resorted to make soft tantalum. Confirmation of the relative differences in plastic deformation will be presented during the discussion of nano-indentation data. Further analyses of the grain size, at the interfaces of both broken and bonded regions (shown in figure and Figure 6), are presented in Figure 8. The data clearly shows that the grains at the wavy region were much finer than bonded region.

The pole figures show the micro textures obtained from the bonded (see Figure 9(a)) and the region where there is excess deformation (see Figure 9(b)). The micro texture of the bonded region showed a Goss texture (see Figure 8(a)), where the $\{110\}$ planes are aligned with the Normal Direction, and the $\langle 100 \rangle$ directions are aligned with the rolling (here vibration) direction. The ideal positions of a Goss Texture are also shown in Figure 9(a). In the case of the sample with broken bond region, the presence of a strong shear component $\{111\} \parallel \text{ND}$ and $\langle 112 \rangle \parallel \text{RD}$ rotated about the normal direction was confirmed. These components are also present in Figure 9(a) in the bonded region and are highlighted with open triangles. This rotation could have occurred as a result of unstable nature Goss texture, which tends to rotate away with increased plastic deformation. The texture developed due to the

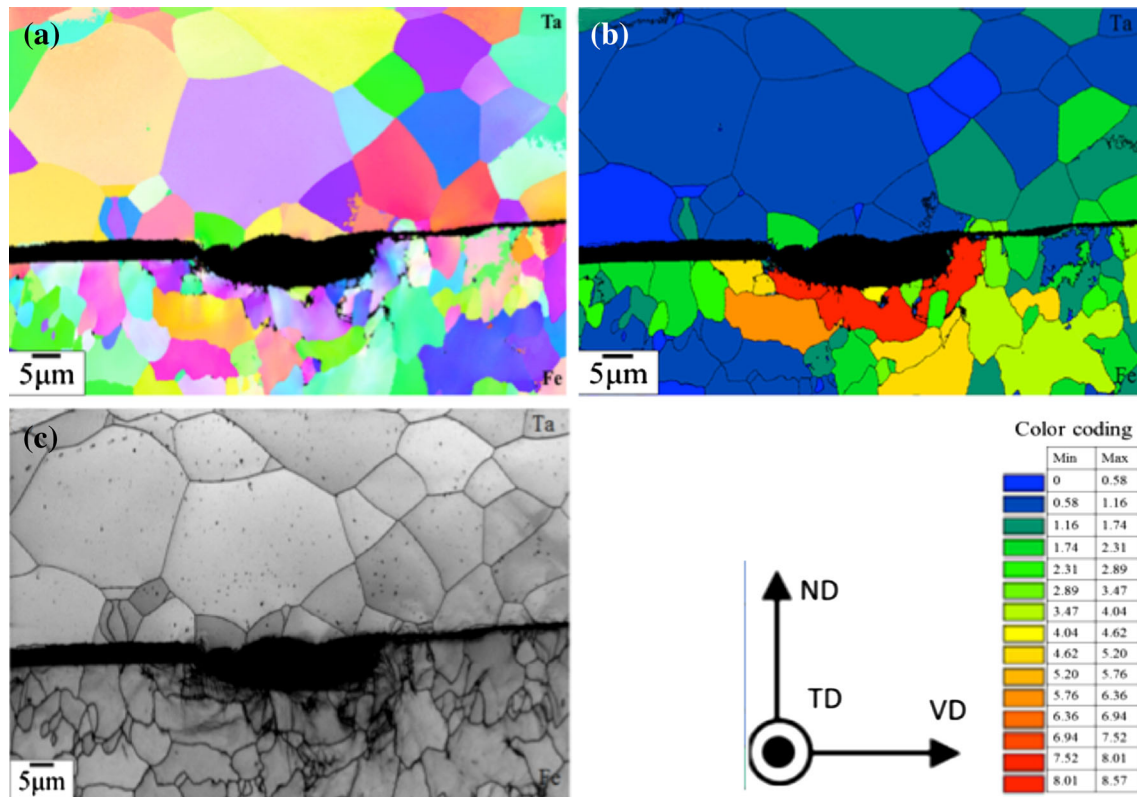


Fig. 5—Microstructural characteristics of the unbonded area. (a) Inverse pole figure of the unbonded region. (b) Grain Orientation spread of the subject region. (c) Image quality index of the corresponding region.

excessive plastic deformation is also slightly stronger (*i.e.*, 14 times than random) than the one was developed at the interface as shown in Figure 9.

The gradual rise in the grain orientation spread from the base metal to the interface shows that lattice rotation is key feature driving the formation of the observed microstructure at the interface. The misorientation data of the selected grains also indicate significant orientation gradients developing within the grain. It has been reported that the rotation of different portions of the original grain towards different stable texture components leads to refinement.^[23] The OIM and the IQI maps in the non-bonded regions did not show any evidence for plastic deformation. The above EBSD analyses confirmed the role of plastic deformation in the bond formation mechanism.

C. Hardness Measurements Using Nano-Indentation

The load vs Indentation plots show the hardness data obtained through nano-indentation near the bonded interface, sonotrode-affected region, and unbonded regions (see Figure 10). Elastic recovery of less than 50 nm shows that the indentation was well beyond the plastic regime of the underlying material. The amount of elastic recovery for the steel at the interface is very high (Figure 10(c)) which could be attributed to high yield strength. For a detailed understanding of the load versus indentation curve the reader is directed to a Reference 24 paper. The data shows higher hardness values near the interface and the Sonotrode-affected regions.

Figure 10(a) shows that the hardness values for Ta at the interface are higher than the bulk equivalent to that of the sonotrode-affected regions. Interestingly, the EBSD analyses also showed significant grain refinement in similar regions. Based on the above, we hypothesize that the Hall–Petch effect leads to an increase in the hardness. The grain size was estimated using the Hall–Petch relation for tantalum that is reported^[15]

$$H = 780 + \frac{690}{\sqrt{d}} \quad [1]$$

where H is the hardness in MPa and d is the grain size in μm . The hardness for Ta near the interface is 3.41 GPa and that of sonotrode-affected region is 3.28 GPa. The grain sizes, which were calculated as per the Hall–Petch relationship was close to 68 and 76 nm at the interface and the sonotrode-affected regions, respectively. This is less than those observed using EBSD. This indicates that the rise in hardness is not exactly driven by grain refinement but dislocation strengthening could also play a role. The grains with a high grain orientation spread at the interfaces suggest that dislocation strengthening could also contribute to the higher hardness rise. This analyses and microstructure data from previous sections confirm that similar deformation and grain refinement mechanisms occur at the interface and sonotrode-affected regions. The regions between the sonotrode-affected region and the interface has similar hardness value irrespective of condition of the interface (*i.e.*, bonded or unbonded). Interestingly, the hardness at the

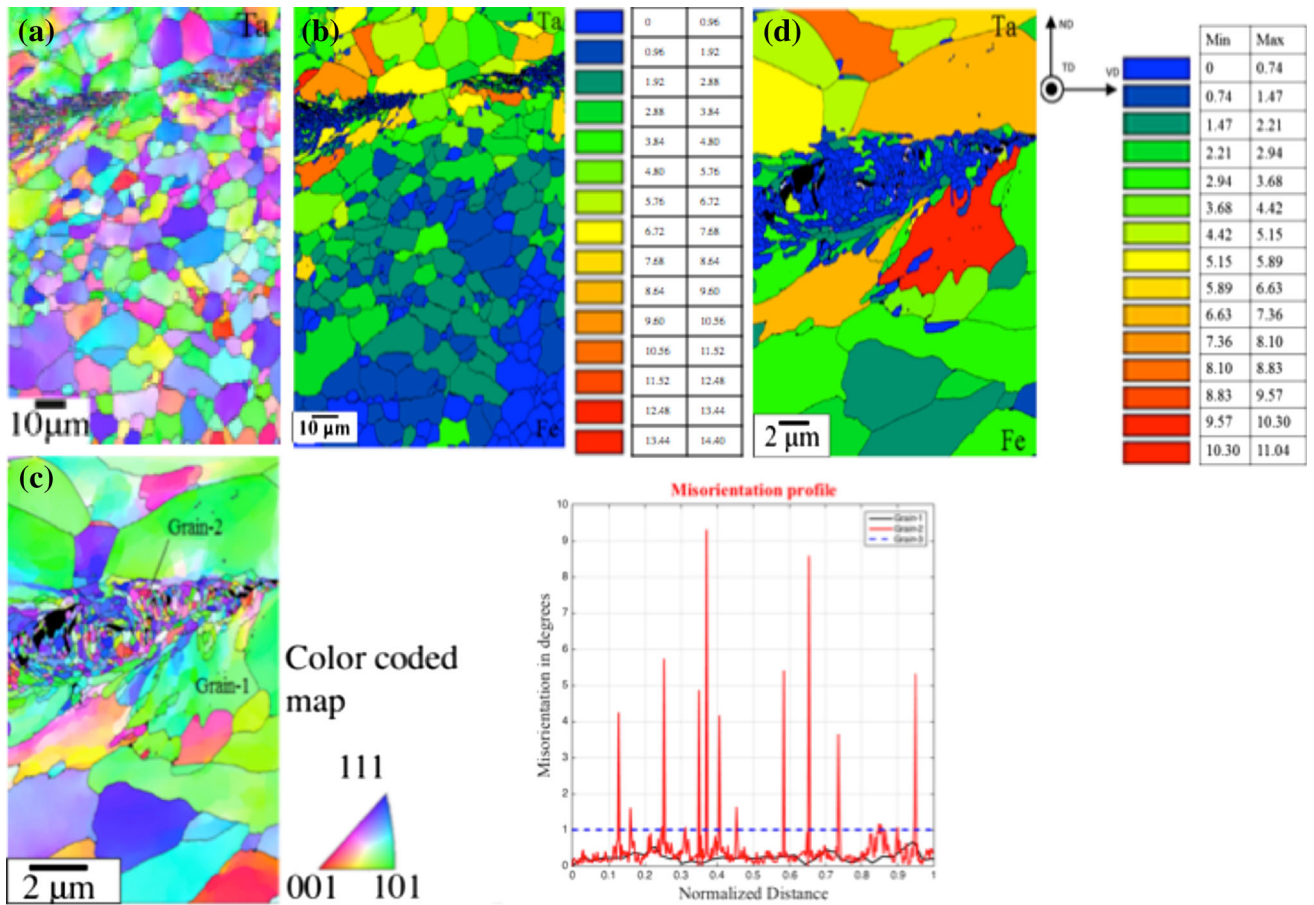


Fig. 6—Microstructural characteristics of the bonded area (a) Inverse pole figure of the bonded region (b) Corresponding GOS (c) IPF of the bonded region in higher mag (d) Corresponding GOS map.

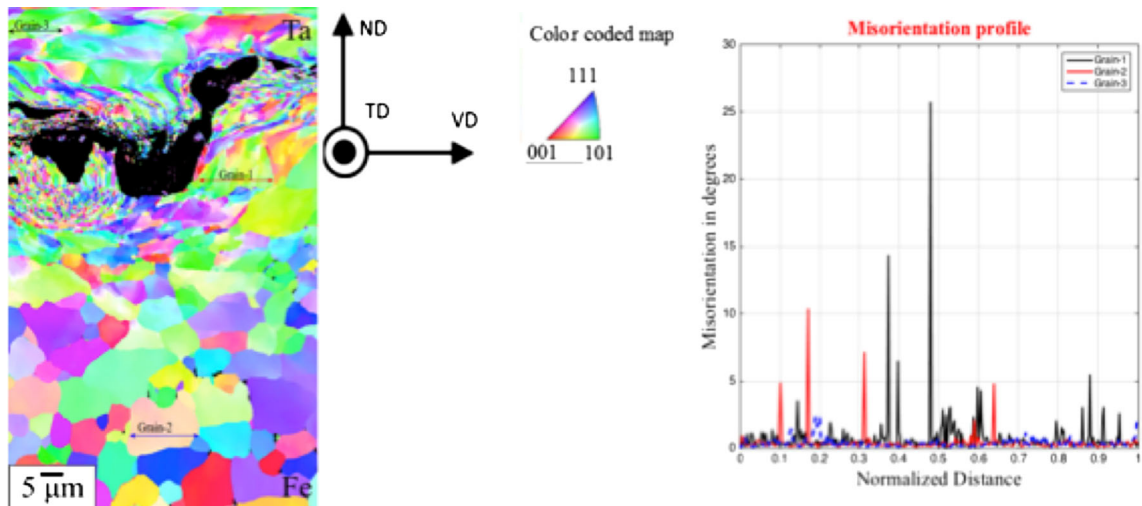


Fig. 7—Microstructural characteristics of a heavily deformed region (a) Inverse pole figure (b) Misorientation distribution for grain-1, grain-2, and grain-3.

sonotrode-affected regions stays almost constant irrespective of the bond formation. At the same time, abetting interfaces at the unbonded regions show a drop

in the hardness, confirming again lack of plastic deformation, thereby proving the significance of plastic deformation at the interfaces. On the steel side, we can

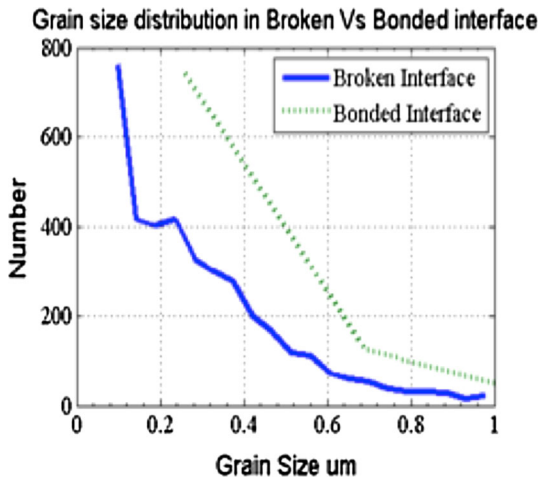


Fig. 8—Grain size distribution in the both the bonded and the broken interface.

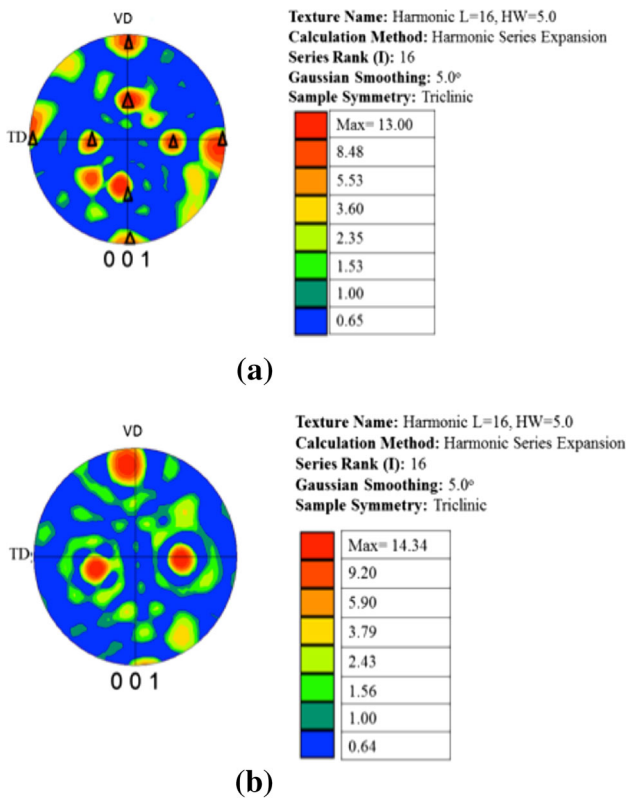


Fig. 9—(a) Texture at the region where bonding was observed (b) micro texture at the region where excess deformation was observed.

see a significant increase in the hardness at the interface regions where the hardness is 5.6 GPa and leveling off at 3.6 GPa as a function of depth from the interface. This confirms the deformation in steel side is concentrated only close to the interface.

The initial region of the load vs displacement curves for Ta shows that curves of the harder regions is identical to that of the softer regions up to a depth of 120 nm and then later on the harder material shows very

high rise in the slope. Also at the unbonded regions, both in the case of steel and Ta, the hardness values were lower and match with the hardness of the bulk. The inhomogeneity of the hardness values across the build, at the interface and sonotrode-affected regions suggest that contact stress of the sonotrode across the build surface is indeed not uniform.

IV. DISCUSSIONS

A. Bond Formation Mechanism During VHP-UAM

From the above results we observe that bonded interfaces have high hardness and refined grain structure with substantial defect density in certain grains (high GOS). To understand the above changes, let us restate three conditions required for solid-state welding; (i) Atomistically clean surfaces; (ii) Intimate contact between nascent surfaces; and (iii) collapse of surface asperities. In order to induce the above conditions, the oxide layers have to be removed completely. In UAM, oxides layers and contaminants are removed as a result of the severe cyclic plastic deformation at the faying surfaces.^[2] The second condition is to bring the surfaces into intimate contact. When a load is applied on the surfaces, the contact points yield allowing for the asperities to flow and induce micro welds. These micro-welds grow as a result of the transverse stresses due to ultrasonic vibrations. Since initial bonding occurs only at the local regions of contact, continued plastic deformation is necessary for the bond to grow by locally extruding the metal into the unbonded regions. We observe islands of micro welds in between bonded and unbonded regions Figure 2. Similar localized micro welds have been observed previously.^[20] This is a result of insufficient plastic deformation adjacent to these micro welds is supported by no change grain structure in the adjoining region. This has been reported elsewhere in Al-Al bonds.^[20] Though the interface is sharp, we observe interpenetration of both Ta and steel near the wavy regions of the interface (Figure 2). These features have been previously reported^[19] and hypothesized to be just mechanical intermixing. This mechanical intermixing is not similar to mechanical alloying that is observed in ball milling, rather due to burying action of wear particles into sub-surface region due to complex asperity collapse and shear deformation. Nevertheless, recent reviews on sliding wear postulate atomic level mechanical mixing of atoms.^[25] As mentioned earlier, the non-homogeneity of bond formation can be attributed to the non-uniform contact pressure distribution and plastic deformation observed both along welding path and across foil width, in agreement with published results from ultrasonic welding.^[4] It is also pertinent to mention that despite the severe plastic deformation occurring in the Ta foil the foil does not bond with the sonotrode due to the following reason. For bond formation in UAM it is imperative that there be a relative motion between the foils. This occurs between the Ta and steel foil but not between the sonotrode and the Ta foil. However, recent

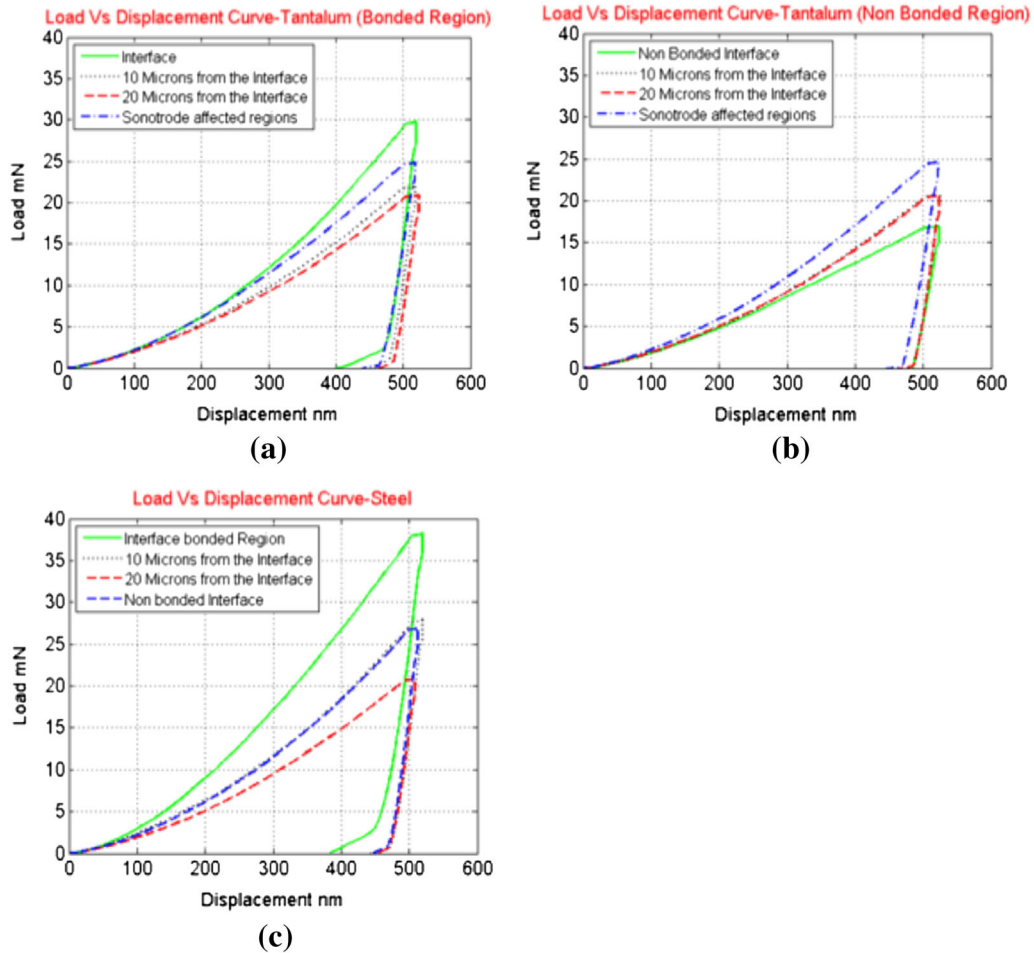


Fig. 10—(a) Load vs displacement curves on the Ta side of the interface (bonded). (b) Load vs displacement curves on the Ta side of the interface (not bonded). (c) Load vs displacement curves on the steel side of the interface.

experiments using photon Doppler velocimetry has shown that after the bonding between the foil and substrate is complete then a relative motion between the top foil and the sonotrode was observed. Thus, when the travel speed is slow and when the energy levels are high we may observe sticking of the foils to the sonotrode.^[26]

However, as stated above a more detailed characterization is necessary to conclude experimentally about the nature of this mechanical mixing that occurs at the interfaces. Wave features (see Figure 2) were observed during ultrasonic spot-welding also^[20] and were attributed to excessive plastic deformation. However, in our case the formation of waves can be understood using the following mechanism outlined by Hopkins *et al.*^[3] with dissimilar Al-Ti welds. In their work, softer Al flowed around the contours of the harder Ti during and therefore no deformation induced was expected. A rough interface is also favorable for explosive welding because surface roughness enhances interpenetration between the two dissimilar materials and also promote frictional heating at the interface, which is essential to bond formation.^[19] It was hypothesized that initial material without asperities would not bond well.^[27] Nano-indentation measurements show that Ta had hardened at the interface possibly due to grain

refinement at the interface. EBSD data also seems to indicate that the bulk of deformation was concentrated on the softer Ta. This may have led to poor oxide removal on the steel surface due to the lack of asperity collapse which brings atomistically clean surfaces which are hypothesized to be required for initiating a solid-state weld where metallurgical bonding can occur.

There are a numerous regions where bonding had not occurred despite extensive plastic deformation observed (Figure 2(b)). One possible reason could be attributed to breaking of the pre-existing bonds. This has been previously observed and reported^[28] where, an increase in amplitude did not correspond to increased strength and linear weld density. This phenomenon was attributed to excessive strain hardening resulting in the bond degradation and rationalized as following. As soon as a weld is established it will be subjected to high frequency ultrasonic vibrations. During each cycle a balance between increase in adhesion and the degradation of the pre-existing bond due the high frequency ultrasonic vibrations may occur. As a result, there is an optimum energy window within which the continued bond formation may occur without breaking the pre-existing or bonds that formed in previous vibration cycles. A less ultrasonic power would result in the lack of

metal-to-metal contact and an increase in the energy would lead to the fracture of the pre-existing bond (see Figure 7(a)). The above hypothesis is supported by OIM data, where the interface shows clear signs of excess plastic deformation by an increased misorientation and associated increase in GOS at the interface grains. Furthermore, the grain size in the broken bond region is much finer than that of bonded interface.

B. On the Evolution of Grain Structure at the Interface

OIM results shown in Figures 6 and 7 do not indicate a uniform equiaxed structure as observed by previous researchers.^[1,2,8,9,29] EBSD of UAM builds carried out by Fuji *et al.* and several others,^[1,8,9] seem to indicate dynamic recrystallization at the bond interface. They attribute the frictional heating during deformation and the high temperature rise due to adiabatic heating to be the driving force for dynamic recrystallization by grain boundary migration to occur.^[1,2,9] In order to explore the possibility of dynamic recrystallization by grain boundary migration in this case it is essential to measure the temperature rise at the interface due to adiabatic heating, which would then be used to understand the kinetics of grain boundary migration at the interface. The rise in temperature is calculated as follows

$$\Delta T = \frac{0.9}{\rho C_p} \int_0^{\epsilon_f} \sigma d\epsilon, \quad [2]$$

where T is the rise in temperature, ρ is the density of Ta (16.53 g/cm³) and C_p of 0.153 J/(g K), σ is the flow stress which in this case is calculated based on the Zerilli Armstrong Equation.^[30]

$$\sigma = C_o + B_o e^{-\beta T} + K \epsilon^n \quad [3]$$

$$\beta = \beta_o - \beta_1 \ln \epsilon', \quad [4]$$

where C_o is the contribution due to lattice friction the second term is the contribution due to strain rate and the third term is the Holloman equation for strain hardening. The values for these constants taken from^[30] are $C_o = 30$ MPa, $B_o = 1110$ MPa, $\beta_o = 0.005$ K⁻¹, $\beta_1 = 0.000327$ K⁻¹, $K = 310$ MPa, and $n = 0.44$. The flow stress obtained from this calculation is integrated over the total strain ϵ_f . The strain was calculated based on the approach outlined by Sriram *et al.*^[9] The asperity height 15 μ m, which was measured based on SEM measurements near regions where the asperity had not collapsed. The shear strain due to lateral displacement of asperities during ultrasonic processing was obtained using the equation (strain = 2 \times amplitude/asperity height). Based on these strain values, we arrive at a temperature rise of 700 K (427 °C) with shear strain equal to 5 and with a shear strain of 10 the temperature can reach 1000 K (727 °C).

These calculations also show that the temperature rise during adiabatic heating is lower than $0.5T_m$. The calculated temperature rise is indeed very sensitive to the strain rate and therefore at regions where the shear

strain exceeds a critical value it is possible to promote recrystallization by grain boundary migration and inter diffusion similar to that of Al-Al bonds. The shear strain is also dependent on the asperity height. It was reported that bonds made on dissimilar metal welds using Al-Cu combinations showed an increase in strength with increase in the surface roughness of the layers. Dynamic recrystallization followed by large grain boundary migration across the faying interfaces cannot occur when the temperature is only 700 K (427 °C). Therefore, we need a different mechanism to explain the observed microstructural features in BCC–BCC dissimilar joints.

Dynamic recrystallization of grains can occur by a continuous and rotational process occurring concomitantly with plastic deformation that leads to sub grain formation which is followed by gradual increase in their misorientation, finally leading to an equiaxed microstructure with high angle grain boundaries. The above process occurs at interfaces with no long-range diffusion. In contrast, migrational dynamic recrystallization occurs by the movement pre-existing high angle grain boundaries of strain-free grains through the deformed microstructure resulting in the overall growth of strain-free grains.^[31] In the current work, the presence of geometrically necessary dislocations that is evident from a GOS value of close to 4 deg at the interface region suggests that migrational dynamic recrystallization may not be operative here, rather rotational dynamic recrystallization might be occurring. Such a mechanism has been observed in adiabatic shear bands of Ta alloys.^[32] Rotational recrystallization is also stated as continuous dynamic recrystallization, which can generate fine-grained structures requires continuous plastic deformation. The dislocations generated during the plastic deformation after reaching a critical level will forms elongated sub grains, which occurs to minimize the strain energy in the lattice. With continuing deformation the sub grains eventually break up into equiaxed grains at the interface and continued rotation increases the misorientation between the grains leading to the HAB's observed at the interface. Continued deformation causes the further refinement of these grains and thus very fine grain distribution, which has resulted in the finer grain structure in Figure 7.

C. On the Texture Evolution at the Interfaces

On close examination of the OIM IPF maps there are certain grains that have a well-developed sub grain structure (and have a high GOS value) at the interface while other grains have a low GOS and no substructure development. This means that the deformation has not resulted in any orientation gradients within the grain itself. This could be rationalized as follows. It has been reported in the literature that the orientation gradient in the grains depends strongly on the ‘Taylor Factor’ which in turn depends initial orientation of the individual crystals.^[33] Taylor Factor corresponds to the ease with which a grain deforms homogeneously. A grain with a low Taylor factor such as the ‘rotated cube orientation’ {001} <110> deforms homogeneously and does not develop sub grains, whereas the {111} <uvw> and {112} <110> (α fiber grains) develop a large orientation

gradient since different regions within the grain deforms by different slip systems.^[34]

The formation of Goss texture where the $\{110\}$ parallel to the ND and the $\langle 100 \rangle$ parallel to the RD normally occurs during recrystallization of the heavily deformed 3 pct Silicon steels or in grains with $\{111\}$ $\langle 112 \rangle$ orientations. The rationale was that of oriented nucleation where the $\{111\}$ $\langle 112 \rangle$ orientation with a high Taylor factor that had formed as a result of severe shear banding had severed as a nucleation site where the Goss grains had nucleated.^[35] However, it had been shown that the Goss texture is a result of static recrystallization.^[35] The Goss texture has also been previously observed as a surface texture in steels when rolling is carried out without any lubrication and the temperature is close to 371 °C where the $\{100\}$ $\langle 110 \rangle$ texture transforms to a $\{110\}$ $\langle 100 \rangle$ texture primarily due to shear at the surface. But other observations have also reported the formation of Goss texture at room temperatures when subjected to a combination of plane strain and shear deformation. The shear deformation tends to stabilize the Goss texture which is unstable under a plane strain condition and rotates to a $\{001\}$ $\langle 110 \rangle$ and $\{111\}$ $\langle 112 \rangle$ texture.^[36] The intense shear deformation at the interfaces in the case of VHP-UAM could have resulted in the formation of a stable Goss texture at the interface. From the adiabatic heating rate calculations it is also clear that the temperatures developed are insufficient to promote static recrystallization at the interface due to short time involved and hence the Goss texture that has developed at the interface is clearly due to the imposed plastic deformation alone. However, in the case of the region where the bonds were hypothesized to be broken the further increased deformation could rotate the Goss texture to a $\{111\}$ $\langle 112 \rangle$ texture as shown previously which is confirmed by the texture shown in Figure 9(b).

Based on the above discussions, we can state that the degree of grain refinement in BCC–BCC UAM joints is predominantly dictated by the amount of plastic deformation also and not due to the adiabatic heating alone, as previously hypothesized.^[4] The initial crystal orientation dictates the degree of subdivision necessary. And on reaching certain stable orientations, the grains do not subdivide further (as seen in EBSD (Figures 6(a) and (c)).^[5] Thus, it is concluded that the grains at the interface had formed by a continuous dynamic recrystallization process which involves grain rotation driven by plastic deformation resulting in the formation of the fine grain structure at the interface.

V. CONCLUSIONS

The present study examined the feasibility of Fe-Ta dissimilar metal combinations using UAM and details of microstructure evolution. Although, successful welds were obtained, the microstructural characterization showed three distinct regions:

1. No mechanical contact: Voids due to lack of any interaction between faying surfaces, as well as low grain orientation spread; the unbonded interface regions are softer than bulk regions

2. Optimum deformation and intimate metal-to-metal contact: Good solid-state bonding, fine interface grains with large misorientation and with Goss texture, that are harder than matrix
3. Excessive deformation: leads to breakage of pre-existing bonds, but still shows fine interface grains with large misorientation spread formed during bonding. These broken regions also exhibit shear texture and are harder than matrix

The above heterogeneity in deformation, changes in crystal texture, and hardness is attributed to the differences in the contact pressure of the sonotrode along these regions, as well as, initial orientation of the grains. Based on the observed observations, we conclude that the well bonded interface regions evolve by continuous plastic deformation, adiabatic heating to temperatures below $0.5 T_m$, subdivision of original matrix grains, followed by grain rotation through a continuous dynamic recrystallization process. The above hypothesis was supported through detailed characterization of textures at the faying interfaces and the calculations of adiabatic heating during high strain rate processing.

ACKNOWLEDGMENTS

This work was carried out as a part of NSF-IUCRC CIMJESA. The authors are grateful to EWI for financial support. The authors also thank The Ohio State University's CEMAS for providing the microscopy facilities to carry out this research work. The contributions of Michael Gram and Professor Peter M. Anderson at The Ohio State University for providing access to the Nano indenter are also acknowledged. The authors also acknowledge Dr. Shibayan Roy at Oak Ridge National Laboratory for very insightful discussions.

REFERENCES

1. R.R. Dehoff and S.S. Babu: *Acta Mater.*, 2010, vol. 58 (13), pp. 4305–15.
2. T. Fujii Hiromichi, M.R. Sriraman, and S.S. Babu: *Metallurg. Mater. Trans. A*, 2011, vol. 42A, pp. 4045–55.
3. C.D. Hopkins, P.J. Wolcott, M.J. Dapino, A.G. Truog, S.S. Babu, and S.A. Fernandez: *Journal of Engineering Materials and Technology*, 2012, vol. 134 (1), p. 011004.
4. M. Kulakov and H.J. Rack: *Mater. Technol.*, 2009, vol. 131 (2), p. 021006.
5. G.D. Janaki Ram, Y. Yang, and B.E. Stucker: *J. Manuf. Syst.*, 2006, vol. 25 (3), pp. 221–38.
6. C. Joshi Kailash: *Weld. J.*, 1971, vol. 50 (12), pp. 840–48.
7. K. Johnson, H.C. Edmonds, R.L. Higginson, and Harris R.A.: in *Proceedings of the Institution of Mechanical Engineers, Part L: Journal of Materials Design and Applications* (2011): 09544207114 13656.
8. D.E. Schick: Dissertation, The Ohio State University, Columbus, 2009.
9. M.R. Sriraman, S.S. Babu, and M. Short: *Scripta Mater.*, 2010, vol. 62 (8), pp. 560–63.
10. Y.S. Sato, H. Kokawa, K. Ikeda, M. Enomoto, T. Hashimoto, and S. Jogan: *Metallurg. Mater. Trans. A*, 2001, vol. 32A, pp. 941–48.

11. D. Raabe, G. Schlenkert, H. Weisshaupt, and K. Lücke: *Mater. Sci. Technol.*, 1994, vol. 10 (4), pp. 299–305.
12. S. Mironov, Y.S. Sato, and H. Kokawa: *Acta Mater.*, 2008, vol. 56 (11), pp. 2602–14.
13. J.F.C. Lins, H.R.Z. Sandim, H.J. Kestenbach, D. Raabe, and K.S. Vecchio: *Mater. Sci. Eng. A*, 2007, vol. 457 (1), pp. 205–18.
14. M.A. Meyers, Y.J. Chen, F.D.S. Marquis, and D.S. Kim: *Metallog. Mater. Trans. A*, 1995, vol. 26A, pp. 2493–2501.
15. Q. Wei, Z.L. Pan, X.L. Wu, B.E. Schuster, L.J. Kecskes, and R.Z. Valiev: *Acta Mater.*, 2011, vol. 59 (6), pp. 2423–36.
16. R.Z. Valiev, Y. Estrin, Z. Horita, T.G. Langdon, M.J. Zechetbauer, and Y.T. Zhu: *JOM*, 2006, vol. 58 (4), pp. 33–39.
17. F. Trueb Lucien: *Metallurg. Trans.*, 1971, vol. 2 (1), pp. 145–53.
18. O.W. Carl and G.M. Pharr: *J. Mater. Res.*, 1992, vol. 7 (06), pp. 1564–83.
19. B.A. Greenberg, M.A. Ivanov, V.V. Rybin, A.V. Inozemtsev, O.V. Antonova, O.A. Elkina, A.M. Patselov, S.V. Kuz'min, V.I. Lysak, and V.E. Kozhevnikov: *Phys. Met. Metallogr.*, 2012, vol. 113 (2), pp. 176–89.
20. R. Jahn, R. Cooper, and D. Wilkosz: *Metallurg. Mater. Trans. A*, 2007, vol. 38A, pp. 570–83.
21. J.Y. Kang, D.I. Kim, K.H. Oh, and H.C. Lee: *Mater. Sci. Forum.*, 2004, vol. 467, pp. 69–74.
22. R.D. Doherty, D.A. Hughes, F.J. Humphreys, J.J. Jonas, D. Juul Jensen, M.E. Kassner, W.E. King, T.R. McNelley, H.J. McQueen, and A.D. Rollett: *Mater. Sci. Eng. A*, 1997, vol. 238 (2), pp. 219–74.
23. D.A. Hughes and N. Hansen: *Acta Mater.*, 1997, vol. 45 (9), pp. 3871–86.
24. W.C. Oliver and G.M. Pharr: *J. Mater. Res.*, 2004, vol. 19 (01), pp. 3–20.
25. D.A. Rigney, L.H. Chen, G. Malcolm, S. Naylor, and A.R. Rosenfield: *Wear*, 1984, vol. 100 (1), pp. 195–219.
26. D.R. Foster, G.A. Taber, S.S. Babu, and G.S. Daehn: *Sci. Technol. Weld. Joining*, 2014, vol. 19 (2), pp. 157–63.
27. X. Changqing and Z. Jin: *Surf. Coat. Technol.*, 2000, vol. 130 (1), pp. 29–32.
28. T. Watanabe, A. Yanagisawa, and S. Sunaga: *Metallurg. Mater. Trans. A*, 2003, vol. 34A, pp. 1107–11.
29. C.Y. Kong, R.C. Soar, and P.M. Dickens: *J. Mater. Process. Technol.*, 2004, vol. 146 (2), pp. 181–87.
30. Z. Frank and R.W. Armstrong: *J. Appl. Phys.*, 1990, vol. 68 (4), pp. 1580–91.
31. B. Derby: *Acta Metallurg. Mater.*, 1991, vol. 39 (5), pp. 955–62.
32. M.T. Perez-Prado, J.A. Hines, and K.S. Vecchio: *Acta Mater.*, 2001, vol. 49 (15), pp. 2905–17.
33. D. Raabe, Z. Zhao, S.J. Park, and F. Roters: *Acta Mater.*, 2002, vol. 50 (2), pp. 421–40.
34. B. Hutchinson: *Philos. Trans. R. Soc. Lond. Ser. A*, 1999, vol. 357 (1756), pp. 1471–85.
35. J.T. Park and J.A. Szpunar: *Acta Mater.*, 2003, vol. 51 (11), pp. 3037–51.
36. S.H. Lee and D.N. Lee: *Mater. Sci. Eng. A*, 1998, vol. 249 (1), pp. 84–90.